



## Experimental investigation of an air gap membrane distillation unit with double-sided cooling channel

Dahiru U. Lawal\*, Atia E. Khalifa

*Mechanical Engineering Department, King Fahd University of Petroleum & Minerals, Dhahran 31261, Saudi Arabia, emails: l.dahiru@yahoo.com (D.U. Lawal), akhalifa@kfupm.edu.sa (A.E. Khalifa)*

Received 15 October 2014; Accepted 9 April 2015

---

### ABSTRACT

Membrane distillation (MD) is a non-isothermal membrane separation process capable of operating at low temperature and low transmembrane hydrostatic pressure. Air gap membrane distillation (AGMD) is one of the MD configurations. In this study, the performance of double-stage AGMD unit at different AGMD-operating parameters such as feed temperature, feed flow rate, coolant temperature, coolant flow rate and air gap width is presented. Experimental results revealed that the built double-stage AGMD unit is capable of achieving a maximum cumulative distillate production of 128.46 kg/m<sup>2</sup>h, a total (average) flux of 64.23 kg/m<sup>2</sup>h and a single-stage flux of 65.81 kg/m<sup>2</sup>h. One key feature of the proposed design is the ability of the unit to use a common cooling chamber to provide the necessary cooling required by the two feed chambers. This reduces the total capital, maintenance and total energy consumption costs. Other benefits include simple module design, easy modules installation and improved system productivity. Furthermore, the system can be operated either as a single-stage or double-stage unit. A simple theoretical model for predicting flux in single-stage AGMD unit was equally presented. The model predicted fluxes with less than 13% discrepancy.

*Keywords:* Desalination; Membrane distillation; Single-stage; Double-stage; Heat and mass transfer

---

### 1. Introduction

The quest for better fresh water production has consistently put researchers in search for superior and most efficient potable water production technology. The emergence of membrane distillation (MD) technology in 1980s had contributed to the research on seawater desalination. Due to urbanization and rise in population, the bridge between the demand and supply of potable water is ever increasing. In some arid

and semi-arid area, desalination remains the only alternative solution to water scarcity problem [1]. Desalination is one of the cost effective and affordable methods of providing solution to the problems of fresh water scarcity [2]. The existing desalination technology has been developed to a point where it can serve as a reliable source of water at a competitive price with that of conventional water treatment technology [3]. Large water body such as sea or ground water reserves are the sites where desalination plants are mostly situated.

---

\*Corresponding author.

Several desalination technologies are available and MD is one of the promising technologies for desalting seawaters. MD is based on the application of vapour pressure differential to permeate water through a hydrophobic membrane, while rejecting the non-volatile compound available in the feed water [4]. The four widely known basic configurations of MD include direct contact membrane distillation (DCMD), air gap membrane distillation (AGMD), sweeping gas membrane distillation and vacuum membrane distillation (VMD). While the design of the feed sides of all these MD configurations remains the same, the design of the cold side of the membrane and the way in which the permeated flux are collected differs for each configuration [5]. In AGMD configuration, the temperature difference between the sides of a hydrophobic membrane material creates partial pressure difference which encourages water molecules to evaporate at the hot feed side to permeate through the pores of the membrane material. The vaporized water then diffuses through a stagnant air gap situated between membrane and cooling plate. The vapour eventually comes in contact with the cooling surface where it condenses at a lower temperature to produce distilled water [6]. The performance of AGMD system is greatly affected by several operating factors which includes feed temperature, feed flow rate and the air gap depth. The influence of coolant temperature on the performance of AGMD unit is relatively low, while the effect of coolant flow rate is negligible [7,8].

The performance of AGMD for aqueous NaCl solution, natural ground water and seawater was experimentally investigated by Pangarkar and Sane [9]. The effect of operating parameters such as feed flow rate, feed temperature, feed salt concentration, coolant temperature and the air gap thickness on the permeate flux was reported and discussed. Result revealed that the permeate flux increases with the increase in feed temperature and feed flow rate. However, it decreases with the increase in coolant temperature and air gap thickness. Scale deposits observed on the membrane surface were said to be responsible for about 23% reduction in permeate flux for ground water and 60% for seawater.

Singh and Sirkar [10] designed, fabricated and investigated experimentally two hollow-fibres-based compact membrane device for AGMD. Hot brine containing 1% NaCl was used as the feed solution. The performances of the modules were investigated for the ranges of feed temperatures, feed flow rate and the cooling flow rate. Higher permeate flux was obtained as a results of higher brine flow rate and higher cooling flow rate which in turn reduces the temperature polarization and cooling side temperature

resistance. It was concluded from the investigation that for a better performance of MD module, an efficient combination of the two different sets of hollow fibres is required.

De Andres et al. [11] studied experimentally a combined MD module and a one-stage multi-effect distiller. The hot brine rejected from the multi-effect distiller was used as the feed solution to the membrane module. Results revealed that the permeate flux from the combine system increases by about 7.5%, while the gain output ratio of the system increased by 10%. The temperature of about 85°C was considered as the optimum operating condition of the feed solution at the evaporator inlet and a circulation flow of about 170 kg/h.

Numerous theoretical analysis of heat and mass transfer of AGMD have been developed and proposed by different researchers. Jönsson et al. [12] developed simple theoretical expressions for heat and mass transfer in AGMD. Investigations were conducted on the effect of membrane parameters on the rate of evaporation and heat loss. Results revealed that the air gap between the cooling surface and the membrane surface significantly reduces the heat lost by conduction. However, air gap thickness has little effect on rate of evaporation.

Liu et al. [13] theoretically and experimentally conducted an investigation on AGMD system. Different aqueous solutions of tap water, salt water, dyed solutions, alkali solutions and acid solutions were used as the feed solution. The effects of feed concentration and the width of the air gap in AGMD module were analysed and discussed. The developed theoretical model was validated against the experimental result. Results showed fair agreement between the experimental findings and the theoretical results.

Tian et al. [14] presented an innovative design of AGMD configuration that is cost-effective and high efficient membrane cell. The new design of AGMD configuration was reported to have significantly enhanced water productivity of the system. The AGMD module was built in such a way the membrane material is in partial contact with the condensation surface. This reduces the additional transport resistance offered by the air gap and as such improves the efficiency of the system. With the feed and coolant temperatures of 77 and 10°C, a maximum permeate flux of 119 kg/m<sup>2</sup>h was recorded.

In order to enhance the performance and specific energy consumption of MD system, Lee and Kim [15] proposed a multi-stage vacuum membrane distillation (MVMD) system which can be connected in series, parallel or mixed. Economic analysis of the system was also presented and discussed in their study. The

mixed MVMD with 20 stages was reported to be the best configuration, producing water of about 3.79 m<sup>3</sup>/d. It also recorded the lowest water production cost and lowest maximum transmembrane pressure difference.

A short-cut design approach to determine the number of identical modules required for extracting maximum heat recovery between inlet and exit feed brine temperature for a cascade structure of cross-flow DCMD was presented by Gilron et al. [16]. The results of their study revealed that lower energy cost may be achieved when we used waste heat from other processes to the DCMD process. Increase in the pressure difference between the saline feed and the condenser maximized flux, however, it results in poor energy recovery. In order to address this problem, Summers and Lienhard V [17] proposed a simple VMD cycle in which many membrane modules and condensers are cascaded at successively lower pressure. The proposed cycle work like multi-stage flash (MSF) desalination systems. In the presented cycle, the flash chambers of MSF systems can be replace with MD modules, which can provide a more compact system, and small-scale and off-grid desalination applications.

Multi-stage membrane distillation has been in existence since the inception of MD process, but no researcher has addressed the flux at each stage in AGMD configuration. Knowing the flux at each stage will provide a better understanding of the trends and the performance of each stage in the system. Thus, the objective of the present study is to design, build and test a simple and effective double-stage AGMD system for water desalination. The proposed design is a similar kind of counter-flow multi-stage AGMD system (without heat recovery). The system provides a means of obtaining permeate flux at each stage. The influence of AGMD-operating parameters on the performance of the newly developed double-stage AGMD module will be investigated. The effect of feed saline concentration on permeate flux will be studied as well. Analysis of heat and mass transfer in a single-stage AGMD will be discussed and validated against the experimental findings. The tested-operating parameters are the feed temperature, feed flow rate, coolant temperature, coolant flow rate and the air gap width.

## 2. Experimental

### 2.1. Material

The membrane material used in this study is polytetrafluoroethylene of 0.45 μm pore size (PTFE 0.45 μm). It is a composite membrane that is composed of an active layer and support layer. The material was

acquired from TISH SCIENTIFIC. The properties of the used membrane material are tabulated in Table 1. The effect of each operating parameters on distillate production was tested using feed solution having total dissolve solids (TDS) of 4.06 g/L, while the effect of salt water concentration was investigated using feed saline water ranging from 0.13 to 30 g/L.

### 2.2. Membrane characterization

Good knowledge of different membrane parameters is needed since they influence the performance of MD separation. In order to determine the membrane parameters, various technique of characterizing MD membrane is required. Membrane characterization was carried out and the main membrane parameters considered in the characterization are the membrane thickness, pore size, porosity and membrane contact angle.

The thickness of the membrane was measured at different points by an electronic micrometer Schut (Schut Geometrical Metrology) and the average values together with their standard deviations are tabulated below.

The mean pore size was measured using a porometer (POROLUX™ 100) that uses a pressure range of 0–0.7 MPa at room temperature. POREFIL 125 (Porometer) was used as a wetting liquid agent. At least, three different measurements were taken and the mean pore size of the tested membrane was reported. The void volume fraction of the membranes was determined by measuring the density of the membrane using isopropyl alcohol at ambient temperature, which penetrates inside the pores and distilled water, which does not. The applied method was reported by Khayet and Matsuura [7]. In this method, a pycnometer and a digital balance, accuracy 0.00001 g, are employed: at least, eight different measurements were performed and the average void volume fraction of the membrane and its standard deviation were calculated and reported. The water

Table 1  
Membrane properties

Properties	PTFE 0.45 μm
$\delta_{full\ membrane}$ (μm)	153.9 ± 13.6
$\delta_{teflon}$ (μm)	6.9 ± 2.0
$\delta_{support}$ (μm)	141.4 ± 15.8
$d_p$ (nm)	379 ± 8
$\varepsilon$ (%)	79.7 ± 8.7
$\theta$ (°) active layer	139.0 ± 2.8
$\theta$ (°) support layer	119.3 ± 1.0



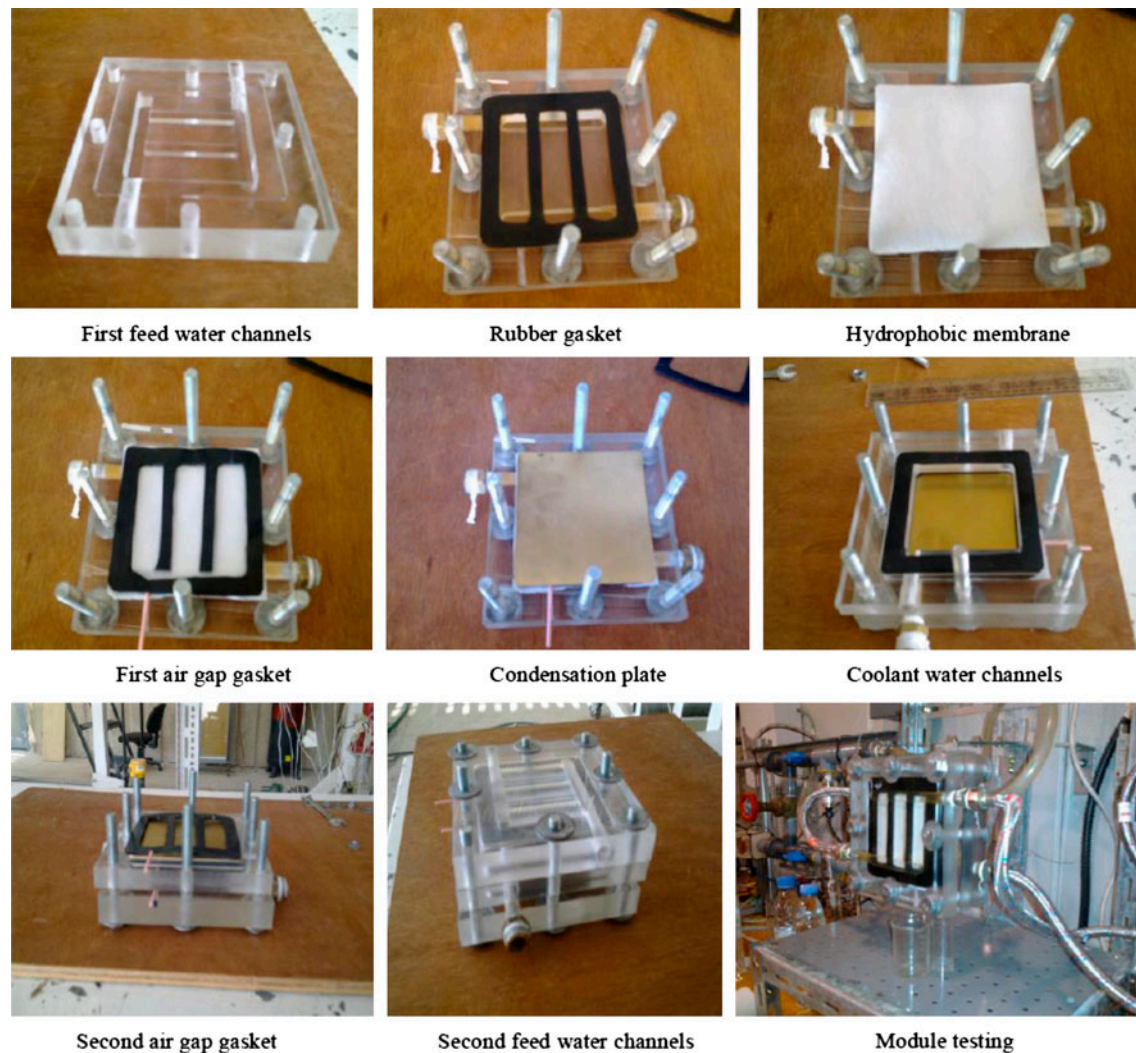


Fig. 2. Module assembling and installation.

rugged pipe plug thermocouple probe (TC-K-NPT-U-72) for measuring the feed and coolant temperatures at the entrances and exits of the module. The TDS and the electric conductivity of the feed saline water and that of the permeated water are measured using Omega CDH-287 conductivity meter. All the measuring devices and sensors are connected to the National Instrument (NI 9234) data acquisition system and all the readings are monitored and stored on a computer using a LabVIEW code.

### 2.5. AGMD system description

The description of AGMD process set-up is as follows: the feed saline water is heated to the required set temperature using a thermostat water bath (model:

HAAKE D8-G) and is pumped to the membrane cell (first stage) using a small centrifugal pump. The hot feed passes over the hydrophobic membrane surface and then exits the first stage to the second stage. The hot water then returned to the hot water bath for reheating and recirculation. Coolant water temperature is controlled and circulated using a refrigerated water bath circulator (model: HAAKE-GH). The cooling water passes over the condensation plate to provide the necessary cooling for vapour condensation. The air gap width is determined and changed by the thickness of the rubber gasket installed between the membrane and the condensation plate. The water vapour generated at the feed channels as a result, vapour pressure difference between both sides of membrane permeates through the membrane pores.

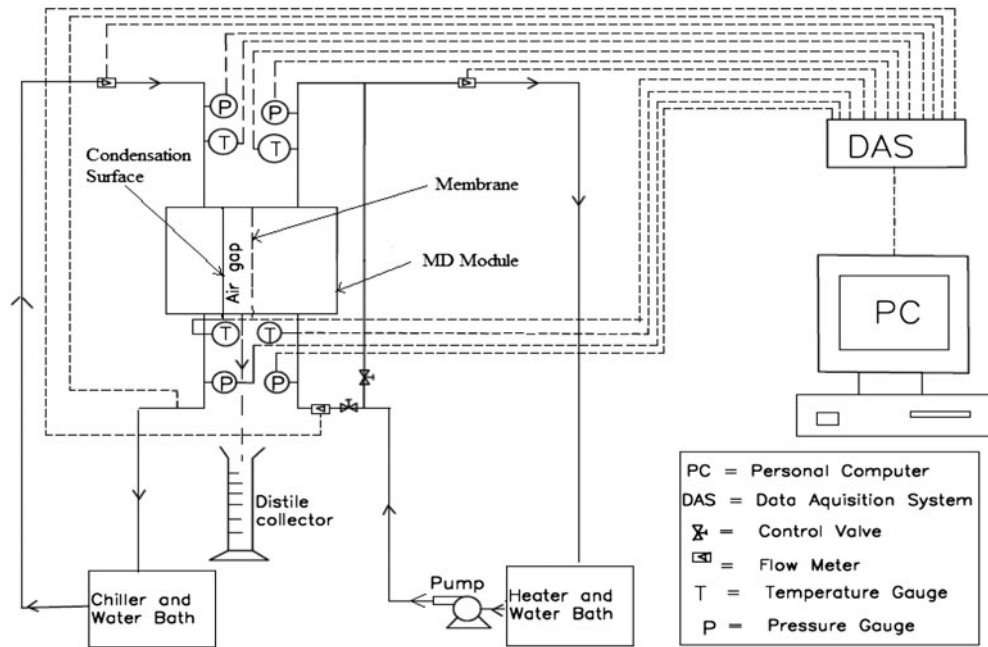


Fig. 3. Schematic diagram of the experimental apparatus.

The vapour then migrates through the stagnant air staged between the membrane sheet and condensation plate. The vapour finally condensed on the condensation surface to form distilled water, and then collected outside the module using a measuring cylinder. The sample time of each experimental data is recorded. The permeate flux was then calculated by dividing the mass of distillate collected by the product of membrane effective area and sample time. The flow diagram of the system is presented in Fig. 4. It is worth mentioning that the MD cell is an integrated single entity. To monitor the performance and salt rejection factor (water quality) of each stage, the distilled water production is collected separately from each stage. Note that at each experimental run, there is an average drop of 2°C in feed temperature between the inlet and outlet of first stage.

### 3. Theory

The schematic diagram of a typical AGMD is illustrated in Fig. 5. The system consists of a microporous hydrophobic membrane sheet situated between hot feed solution and the cooling surface. The cooling surface is in direct contact with the cooling solution which provides the necessary cooling needed by the system. In AGMD configuration, both heat and mass transfer takes place simultaneously across the membrane. The mass transfer across the membrane

depends on the vapour pressure difference between both sides of the membrane. The relationship between mass transfer and water vapour pressure difference can be expressed as [7,13]:

$$J_w = B_w(P_{mf} - P_{cd}) \tag{1}$$

where  $P_{mf}$  is the vapour pressure at the feed side of the membrane, while  $P_{cd}$  vapour pressures at the condensation surface.  $J_w$  is the mass transfer and  $B_w$  is the overall mass transfer coefficient.

The vapour pressures ( $P_{mf}$  and  $P_{cd}$ ) in (Eq. 1) can be evaluated from the Antoine equation at temperatures  $T_{mf}$  and  $T_{cd}$ , respectively. The respective Antoine equations are expressed as:

$$P_{mf} = \exp \left( 23.328 - \frac{3,841}{T_{mf} - 41} \right) \tag{2}$$

$$P_{cd} = \exp \left( 23.328 - \frac{3,841}{T_{cd} - 41} \right) \tag{3}$$

For feed solution containing dissolve salt,  $P_{mf}$  may be estimated from Raoult's law given as [6,18]:

$$P_{mf} = (1 - CM_{NaCl})P_m \tag{4}$$

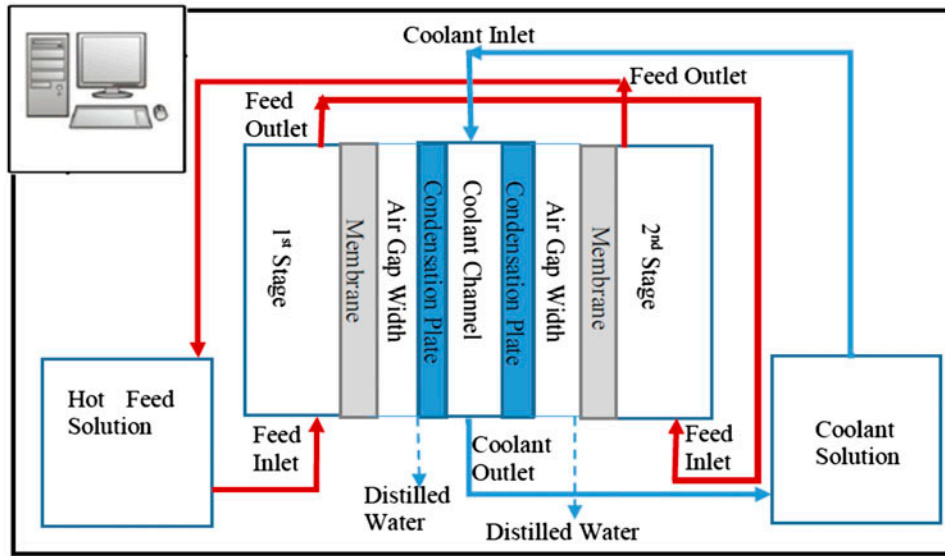


Fig. 4. Flow diagram of two-staged AGMD Module.

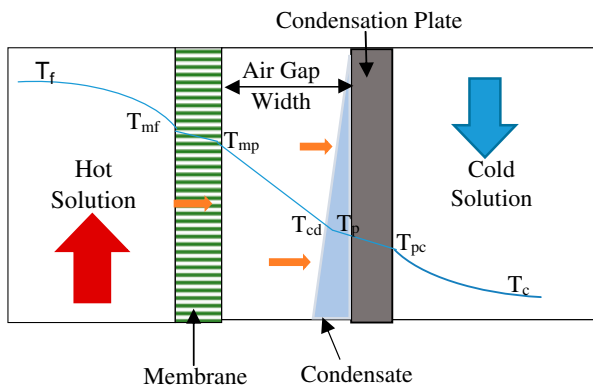


Fig. 5. Model of heat and mass transfer in the AGMD.

where CM = mole solute concentration.

The overall mass transfer coefficient also known as membrane permeability is given as [4,7]:

$$B_w = \frac{\varepsilon P D_{ia}}{RTb'|P_a|_{\ln}} \quad (5)$$

where  $\varepsilon$  is the membrane porosity,  $P$  is the total pressure inside the pore,  $D_{ia}$  is the air diffusion coefficient,  $R$  is the gas constant,  $T$  is the absolute temperature,  $b' = \delta\tau + b$ ,  $\delta$  is the membrane thickness,  $\tau$  is the membrane tortuosity,  $b$  is the air gap thickness and  $|P_a|_{\ln}$  is the log mean air pressure expressed as:

$$|P_a|_{\ln} = \frac{(p_{amf} - p_{acd})}{\ln\left(\frac{p_{amf}}{p_{acd}}\right)} \quad (6)$$

The membrane tortuosity can be obtained from the expression suggested by Macki-Meares [4,19]:

$$\tau = \frac{(2 - \varepsilon)^2}{\varepsilon} \quad (7)$$

To obtain the temperatures  $T_{mf}$  and  $T_{cd}$  needed in Antoine equation, we have to consider the following analysis of heat transfer. Generally, there are two major mechanisms of heat transfer taking place in MD. The first one is the conduction heat transfer across the membrane material, whereas the second one is the latent heat of vaporization that accompanied the mass transfer through the membrane pores. For heat transfer analysis in AGMD process, the following general steps arranged in a preceding order are considered:

- (1) The convection heat transfer from the bulk feed solution to the membrane surface.
- (2) Heat transport by conduction across the membrane material and mass transfer of vapour via the membrane material.
- (3) The conduction heat transfer through the stagnant air gap and heat of condensation at the condensate surface.
- (4) Heat transfer by conduction through the cold plate and

- (5) Heat transfer by convection between the cooling surface and the cooling water.

At steady state, the heat transfer from the hot solution to the membrane surface is given as [8,20]:

$$Q_f = h_f(T_f - T_{mf}) + J_w C_f(T_f - T_{mf}) \quad (8)$$

where  $h_f$  and  $C_f$  are the heat transfer coefficient and the specific heat of the feed solution respectively.

The heat transfer from membrane surface to the condensate liquid interface is expressed as:

$$Q_p = h(T_{mf} - T_{cd}) + J_w H_w \quad (9)$$

where  $H_w$  is the heat of vaporization of water which may be estimated from  $H_w = 1.75535T + 2,024.3$ , where  $T$  is the absolute temperature in K and  $h$  is heat transfer coefficient and its given as [7,8]:

$$h = \left( \frac{J_w C_{cd}}{1 - e^{-\frac{J_w C_{cd}}{h_y}}} \right) \quad (10)$$

$C_{cd}$  and  $h_y$  are the specific heat and the coefficient of heat transfer coefficient in the gaseous phase but  $h_y = \frac{k}{l}$ , where  $k$  is the gas phase thermal conductivity.

The heat transfer from condensation layer interface to the cooling solution is expressed as [7]:

$$Q_c = h_d(T_{cd} - T_p) = \frac{k_c}{l}(T_p - T_{pc}) = h_c(T_{pc} - T_c) = h_p(T_{cd} - T_c) \quad (11)$$

where  $h_d$  is the heat transfer coefficient of the condensate,  $k_c$  is the condensate plate thermal conductivity,  $l$  is the plate thickness,  $h_c$  is the heat transfer coefficient of coolant film and  $h_p$  is the overall heat transfer coefficient from vapour/condensate liquid interface to cooling solution and it is expressed as:

$$h_p = \left( \frac{1}{h_d} + \frac{l}{k_c} + \frac{1}{h_c} \right)^{-1} \quad (12)$$

And

$$h_d = \left( \frac{g \rho^2 H_w k_p^3}{L \mu_d (T_{cd} - T_p)} \right)^{\frac{1}{4}} \quad (13)$$

where  $\rho$ ,  $k_p$  and  $\mu_d$  are the fluid density, thermal conductivity and dynamic viscosity at the condensate film temperature, respectively,  $L$  is the height of air gap and  $g$  is the acceleration due to gravity.

Combination and manipulation of (Eqs. 8–12) lead to

$$T_{mf} = T_f - \frac{H}{h_f} \left( (T_f - T_c) + \frac{J_w H_w}{h} \right) \quad (14)$$

$$T_{cd} = T_c + \frac{H}{h_f} \left( (T_f - T_c) + \frac{J_w H_w}{h} \right) \quad (15)$$

where

$$H = \left( \frac{1}{h_f} + \frac{1}{h} + \frac{1}{h_p} \right)^{-1} \quad (16)$$

The heat transfer coefficients ( $h_f$  and  $h_c$ ) may be estimated from the empirical correlation of the dimensionless numbers expressed as [4,7]:

$$Nu = 1.86 \left( Re Pr \frac{d}{L} \right)^{0.33} \quad (17)$$

where  $Nu$  is the Nusselt number and it is given by  $Nu = \frac{hd}{k}$ ,  $Pr$  is the Prandtl number expressed as  $Pr = \frac{\mu C_p}{k}$ , and  $Re$  is the Reynolds number given by  $Re = \frac{\rho u d}{\mu}$  and  $d$  is the channel hydraulic diameter. Note that the expression given in (Eq. 17) is valid for laminar flow only.

#### 4. Results and discussion

The purpose of the experiments here is to investigate the performance of the developed lab-scale double-staged AGMD system at different system operating parameters. The permeate flux obtained from each stages (first and second stages) and the total permeate flux (total productivity) are presented and commented upon. The total permeates flux is calculated as:

$$J_T = \frac{A_{e1} J_1 + A_{e2} J_2}{A_{e1} + A_{e2}} \quad (18)$$

where  $J_T$ ,  $J_1$ , and  $J_2$  are the total, first stage and second stage fluxes, respectively. While  $A_{e1}$  and  $A_{e2}$  are the membrane effective area in stage one and stage two, respectively. Since the membrane effective area in the

first and second stages is equal, then (Eq. 18) reduces to:

$$J_T = \frac{J_1 + J_2}{2} \quad (19)$$

which is basically the average flux of the two stages.

#### 4.1. Effect of feed temperature

The role of feed inlet temperature on the permeate flux produced for single and double stages is illustrated in Fig. 6. Feed temperature was varied from 40 to 80°C. The data are collected at coolant temperature of 20°C, feed flow rate of 3 L/min, coolant flow rate of 3 L/min, feed concentration of 4.06 g/L and air gap thickness of 3 mm. It can be observed that increase in the feed temperature leads to an exponential rise in the permeate flux. In first stage for instance, increase in the feed temperature from 40 to 80°C leads to about 560% rise in distillate production. This may be due to a reason best explained by Antoine equation (see Eq. 2). According to the Antoine equation, the effect of temperature on vapour pressure is marginally low at lower temperature, but becomes very significant at higher temperature. The higher vapour pressure as a driving force significantly enhanced the performance of the system at higher temperature. As noticed from Fig. 6, the permeate flux production from the first stage is slightly higher than that of second stage by about 1.2 times. This is attributed to the temperature drops (about 2°C) between the first stage and the second stage as a result of conduction heat loss through the membrane material and to the surrounding. The cumulative amount of permeate flux from both stages can be twice that of first stage and more than twice that of second stage. Of course, this is true for lab-scale testing only.

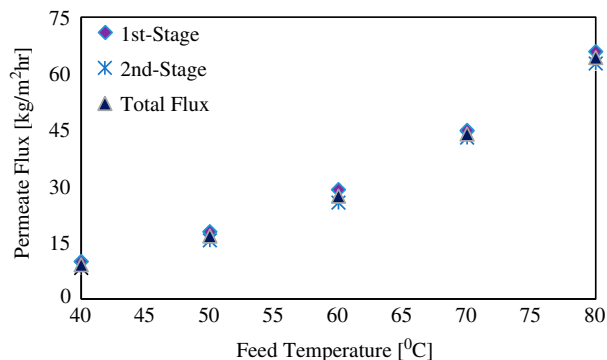


Fig. 6. Effect of feed temperature on permeate flux.

Furthermore, the system total permeate flux due to basing on per membrane area is less than that of first stage and slightly higher than that of the second stage. Although, the productivity from the first stage module is similar to that of the total permeate flux of the two stages. However, the inlet feed temperature of feed stream in the first stage is higher than that of the two-stage system. This is an indication that the single-stage module has a lower productive rate and higher energy consumption. Therefore, comparing the energy input with system productivity, one will ascertain that multistaging the MD system is essential for efficient energy usage.

#### 4.2. Effect of coolant temperature

Coolant temperature is another operating parameter whose impact cannot be ignored because operating the AGMD system at inappropriate coolant temperature will definitely affect the production rate of the AGMD system. Hence, the need for appropriate range of coolant temperature at which maximum possible permeate flux production can be attained thereby arises. In order to investigate the influence of coolant temperature on the performance of the system, coolant temperature was varied from 15 to 30°C, at feed inlet temperature of 70°C, feed flow rate of 3 L/min, coolant flow rate of 3 L/min, feed concentration of 4.06 g/L and air gap thickness of 3 mm. The obtained result is illustrated in Fig. 7. In general, reduction in permeate flux was observed when coolant temperature increases from 15 to 30°C. By increasing the coolant temperature from 15 to 30°C, there is average of about 10% drops in distillate production of each stages. This is due to reduction in transmembrane driving force responsible for permeating the flux. In a nutshell, increase in the coolant temperature decreases the temperature difference between the feed and coolant chambers, this

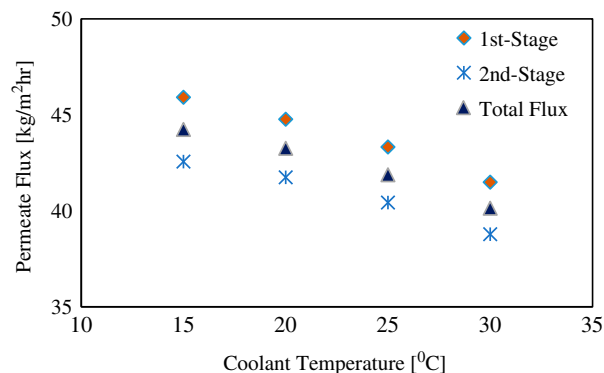


Fig. 7. Coolant temperature as a function of permeate flux.

decline the driving force, hence the observed drops in permeate flux. Using cooling water at atmospheric condition is advisable in this context, since the system performance could only be increased to about 10% when coolant temperature is reduced from 30 to 15°C. This will lower the cost of energy consumption for maintaining the coolant temperature below the room temperature.

It can also be observed that the permeate flux from the first stage is higher than that of the second stage; this is due to 2°C drops in feed temperature between the inlet and exit of the first stage. It must be pointed that the coolant temperature is fairly stable at each experimental run as there is an average +1.2°C rise in coolant temperature. This happened perhaps as a result of using common cooling channel for double staging, which indicate higher heat exchanged between the feed stream and the cooling solution.

#### 4.3. Effect of feed flow rate

Fig. 8 illustrates the influence of hot feed flow rate on distillate production. While keeping feed inlet temperature at 70°C, coolant temperature at 20°C, coolant flow rate at 3 L/min ( $Re = 243$ ), air gap at 3 mm width and using feed solution of 4.06 g/L, the feed flow rate was varied from 1 to 5 L/min (corresponding to  $Re = 81$ –406). It is obvious that higher distillate production rate is obtained at higher feed flow rate. Increase in the feed flow rate from 1 to 5 L/min leads to about 30% rise in flux at each stage. The rise in flux is due to reduction in temperature and concentration polarization effect which decrease the system production. Additionally, increase in feed flow rate encourage turbulent flow level at the feed channels and improved the heat transfer coefficient of the feed boundary layer. Reduction in water residence time in

the module, which relatively increases the feed average temperature, may just be another reason for the observed rise in the permeate flux. The impact of feed flow rate on permeate flux is observed to be greater than that of coolant temperature. Therefore, running the system at higher feed flow rate is desirable in this context. However, precaution must be observed when running the system at higher feed flow rate in order to avoid membrane pore wetting. It must be pointed out that we could not reach the optimum feed flow rate at which the system performance become constant, irrespective of further rise in feed flow rate. Similar to previous observations, the obtained result for the first-stage unit is slightly higher than the second stage.

#### 4.4. Effect of coolant flow rate

Presented in Fig. 9 is the influence of increase in coolant flow rate on the permeate flux. The coolant flow rate was increased from 1 to 3.5 L/min (corresponding to  $Re = 81$ –284). The test conditions are feed temperature of 70°C, coolant temperature of 20°C, feed flow rate of 3 L/min, feed concentration of 4.06 g/L and air gap thickness of 3 mm. Coolant flow rate is observed to have the low effect on the permeate flux in both stages. The essence of higher coolant flow rate is to reduce the air condensate interfacial temperature [7]. This indicates that increase in cooling stream flow rate can lead to a higher cooling water heat transfer coefficient of the cooling surface.

However, it can be observed that coolant flow rate is not sensitive to permeate flux in any of the stages. This means that increase in the coolant flow rate is a waste of energy as far as we have enough streams in the module to conduct away the heat transfer to the cooling surface. In fact, it has been reported by many

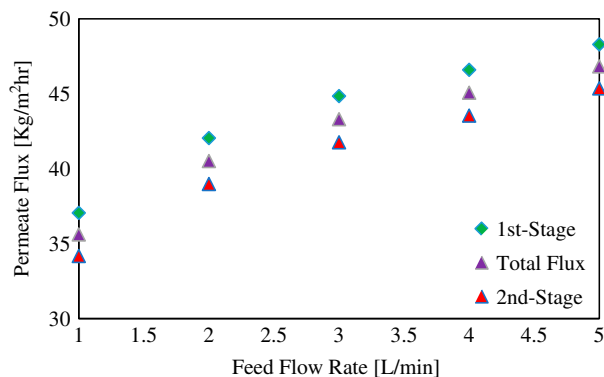


Fig. 8. Effect of feed flow rate on permeate flux.

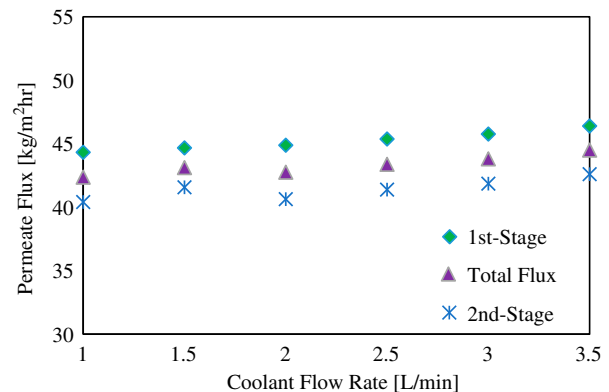


Fig. 9. Coolant flow rate as a function of permeate flux.

researchers including [7,21] that coolant temperature has marginal effect on system performance. In order to reduce cost of quality water production using AGMD, it is advisable to run the system at low flow rate (indicating less input energy demand for pumping). It is worth noting that coolant flow rate significantly affect the performance of DCMD system because of higher heat transfer coefficient rate owing to the direct contact of cooling stream with the membrane.

#### 4.5. Effect of air gap width

Due to mass transfer resistance in the air gap, the thickness of air gap significantly affects the production rate of the system. To investigate the impact of air gap width on the permeate flux, the air gap thickness of 3, 5, and 7 mm is considered. This investigation is conducted at feed temperature from 40 to 80°C, coolant temperature of 20°C, feed flow rate of 3 L/min, coolant flow rate 3 L/min and feed concentration of 4.06 g/L. The results are presented in Fig. 10(a)–(d).

It can be noticed that decrease in the air gap width from 7 to 3 mm at different feed inlet temperature

resulted in considerable rise in distillate production at each stage especially at higher feed temperature. The mean rise in permeate flux is about 130% when air gap width is reduced from 7 to 3 mm in both stages. The reason for this may be attributed to increment in temperature gradient within the vapour compartment as a result of decline in resistance to mass transfer. It is obvious that at each air gap width, water production rate from first stage is higher than that of second stage. The total production rate is observed to be higher than the second stage and lower than the first stage. Since air gap width significantly affects the permeate flux, then it is recommended to use the lowest possible air gap within the module design in order to significantly enhance the performance of the system. Air gap width is considered to be one of the dominant factors affecting fresh water production in AGMD system after feed temperature.

#### 4.6. Effect of feed concentration

One other factor affecting the performance of MD system is the feed saline concentration. To study this effect, an experiment was conducted at coolant

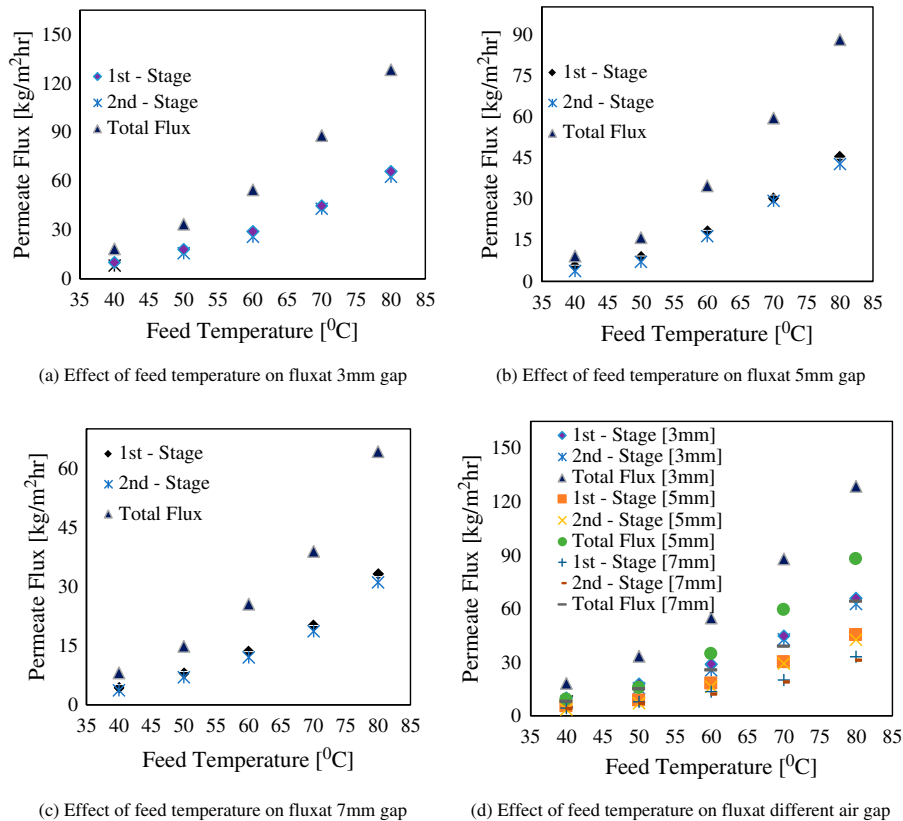


Fig. 10. Effect of air gap thickness on permeate flux.

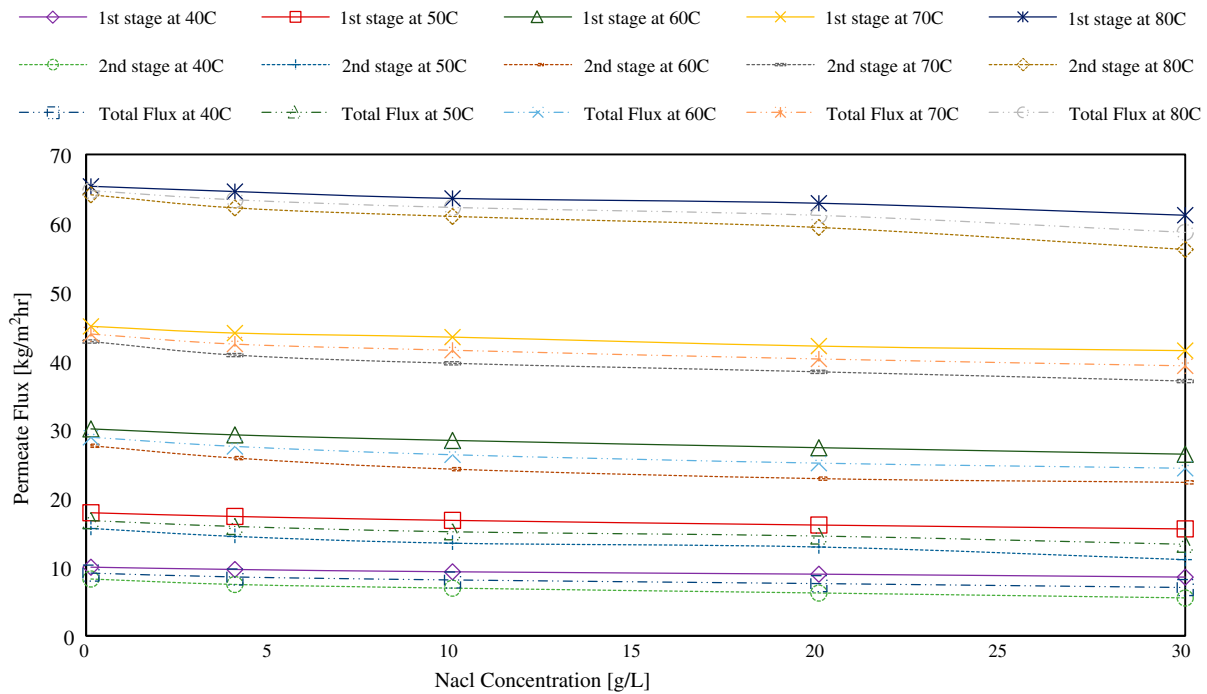


Fig. 11. Variation of permeate flux with feed concentration at different feed inlet temperature (first stage, second stage, and total flux).

temperature of 20°C, feed flow rate of 3 L/min, coolant flow rate of 3 L/min and air gap width of 3 mm. The influence of feed concentration on distillate production at feed inlet temperature ranging from 40 to 80°C was investigated. Fig. 11 represents the variation of hot feed saline concentration against the distil water production of first stage, second stage and total flux. In each case, the production rate tends to decrease slightly with increase in the feed saline concentration. The observed reduction in permeate flux is due to the combine effect of concentration polarization, decreases in water vapour pressure and temperature polarization effect [22]. The addition of non-volatile solutes to water creates additional concentration boundary layer near the feed membrane surface. This decreases the partial vapour pressure of the system and consequently reduces the driving force of the system. Concentration polarization decreases the permeate flux and increases the risk of membrane pore wetting. However, the effect of concentration on flux in MD processes is not significant when compared to temperature polarization effect which leads to the development of film on the feed side membrane surface.

Based on the presented results, increase in the feed concentration from 0.13 to 30 g/L at 60°C feed temperature decrease the permeate production rate by

about 16% at each stage. Careful observation revealed that the effect of feed concentration on flux is becoming less with increase in feed temperature. This is may be due to the fact that at higher feed temperature, water vapour is generated at a faster rate, leaving behind more concentrated solution which affects the system production rate. The obtained results also revealed that the effect of feed concentration on system productivity at the second stage tends to be slightly greater than that of the first stage. This additional effect may be due to increase in feed saline concentration in the first stage before entering the second stage. Unlike pressure driven reverse osmosis, MD can be used to treat a highly concentrated solutions without suffering major reduction the system productivity [6,23]. It must be mentioned that throughout the experiments, the salt rejection factor was found to be 99.98% and above.

#### 4.7. Model results

In order to validate the presented theoretical model, comparisons were made between the model results and the experimental findings at different AGMD operating parameter. Presented in Fig. 12(a)–(e) are the model results against the experimental data. Fig. 12(a) presents the variation of feed temperature as

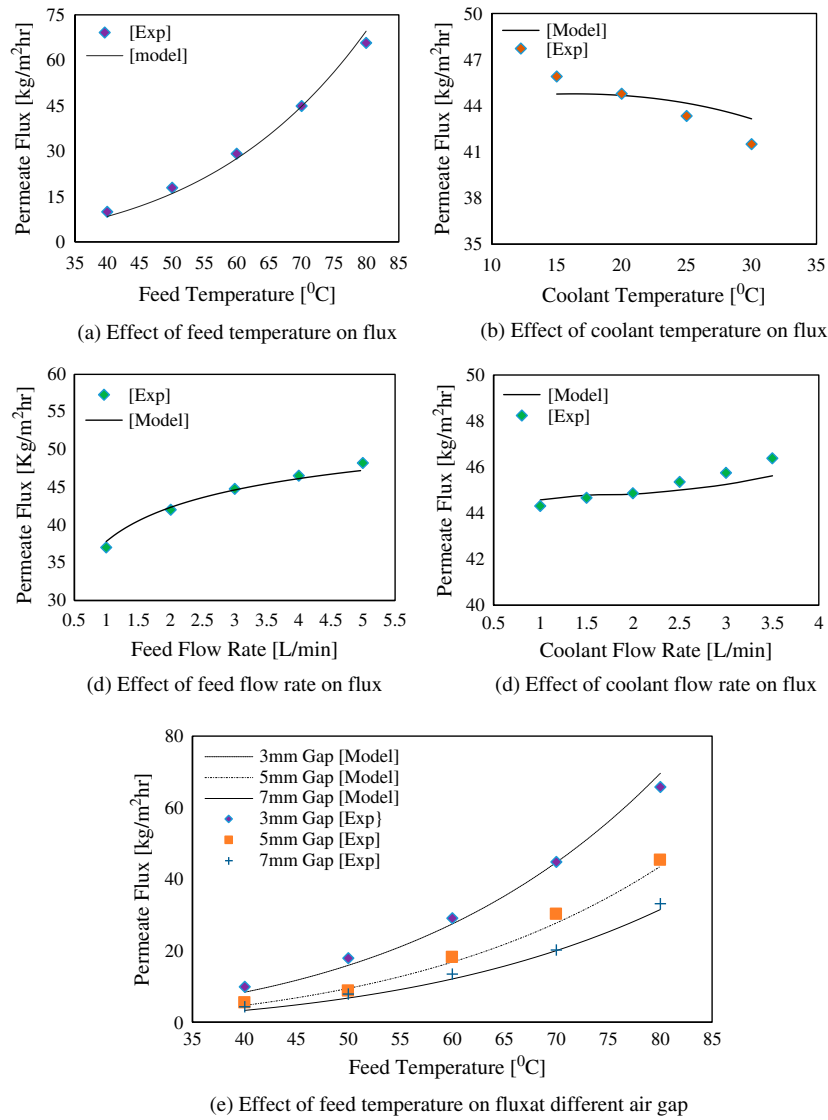


Fig. 12. Model Validation against Experimental data.

a function of permeate flux at coolant temperature of 20°C, feed flow rate of 3 L/min and coolant flow rate of 3 L/min; Fig. 12(b) illustrates the variation coolant temperature as a function of permeate flux at feed inlet temperature of 70°C, feed flow rate of 3 L/min and coolant flow rate of 3 L/min; Fig. 12(c) presents the influence of feed flow rate on permeate flux at feed inlet temperature of 70°C, coolant temperature of 20°C and coolant flow rate of 3 L/min; Fig. 12(d) shows the effect of coolant flow rate on permeate flux at feed temperature of 70°C, coolant temperature of 20°C and feed flow rate of 3 L/min; while Fig. 12(e) illustrates the impact of air gap thickness on permeate flux at different feed temperature ranging from 40 to 80°C.

Coolant temperature of 20°C, feed flow rate of 3 L/min and coolant flow rate 3 L/min are the other conditions.

Careful observation of each figure revealed that the model is better in predicting feed temperature, feed flow rate and air gap width. However, it fails to achieve excellent predictions in the case of coolant temperature and coolant flow rate. In general, the model prediction is considered very good as it is able to predict most of the experimental data. Thus, it has the capability of predicting flux in AGMD system. Analysing the percentage error in each figure, it can be observed that the maximum recorded percentage error between the model results and the experimental data is about 12% when predicting flux at different

feed temperature. This occurred at feed temperature of 50°C. The model was found to predict better between 60 and 70°C. For the flux prediction at different coolant temperature, the maximum model deviation from the experimental data is about 4%. It can also be noticed from Fig. 12(b) that the model accuracy decreases with increase in coolant temperature. For the effect of feed flow rate on permeate flux, the model percentage deviation is within 3% of the experimental data. The model was found to be over predicts at lower feed flow rate and under predict at higher feed flow rate. It can also be observed from Fig. 12(c) that the best model prediction is between 2 and 4 L/min. While for the case of coolant flow rate, the model accuracy is within 2% of the experimental data. From the foregoing discussion, it is obvious that the model prediction is within 12% of the experimental data. We must understand that the discussed model can only predict single (first) stage module. For flux predictions at different air gap width, the maximum percentage error recorded between the model results and the experimental data at 3, 5 and 7 mm gap are about 12, 15 and 21%, respectively. This indicates that the model prediction capability decreases with increase in air gap width. It is worth mentioning that the model does not consider the effect of natural convection in the air gap region. In the model, we assumed that transport of vapour across the air gap is by diffusion. At 3, 5 and 7 mm gap for instance, the calculated Rayleigh number ( $Ra$ ) was found to be 87.66, 422.3 and 1,180, respectively.

For  $Ra$  less than 1,000, natural convection is negligible compared to heat conduction across the gap [24]. So, the effect of natural convection may be responsible for the higher discrepancy between the model and the experimental data at 7 mm gap.

## 5. Conclusions

A parametric study of double-staged AGMD system at different operating parameters including feed inlet temperature, coolant temperature, feed flow rate, coolant flow rate and air gap width has been presented. The impact of feed concentration on the distil water production was as well investigated. Additionally, theoretical model for predicting flux in a single-staged AGMD was discussed. The presented theoretical model was successfully implemented using Matlab code and was validated against the experimental findings.

Based on the presented work, the following conclusions can be drawn from the analysis: The system performance was observed to increase with increase in

feed temperature and feed flow rate. However, it decreases with increase in coolant temperature, air gap thickness and feed saline concentration. The impact of coolant flow rate on the amount of distil water production was observed to be marginal. The maximum first stage, second stage, total and cumulative permeate fluxes obtained from the system were found to be 65.81, 62.65, 64.23 and 128.46 kg/m<sup>2</sup>h, respectively. These were obtained at the feed temperature of 80°C, coolant temperature of 20°C, feed flow rate of 3 L/min, coolant flow rate of 3 L/min, feed concentration of 4.06 g/L and air gap width of 3 mm. Based on the above reported fluxes on the performance of the system, it can be inferred that multi staging the MD system is essential for efficient energy usage and high system productivity. The theoretical model result was observed to be generally in good agreement with the experimental findings. The agreement between the model and the experimental results is quite good as most of the predicted results are within 12% of the experimental data for the air gap width of 3 mm. Hence, the presented model is capable of predicting flux in single stage AGMD system.

## Acknowledgments

The authors would like to appreciate the support received from King Fahd University of Petroleum & Minerals (KFUPM) under the funded project # IN121043.

## Nomenclatures

$B$	— air gap thickness [m]
$C_p$	— specific heat capacity [kJ/kg.K]
$d$	— diameter [m]
$d_h$	— hydraulic diameter [m]
$D_{ia}$	— diffusion coefficients of water vapour in air [m <sup>2</sup> /s]
$g$	— gravitational acceleration [m/s <sup>2</sup> ]
$h$	— heat transfer coefficient [W/m <sup>2</sup> .K]
$h_d$	— condensate film heat transfer coefficient [W/m <sup>2</sup> .K]
$H_v$	— heat of vaporisation [kJ/kg]
$J_w$	— permeate flux [kg/m <sup>2</sup> .s]
$K$	— thermal conductivity [W/m.K]
$B_w$	— mass transfer coefficient [kg/m <sup>2</sup> h Pa]
$l$	— thickness of the cooling plate [m]
$L$	— height of the cooling plate [m]
$M$	— molecular weight [kg/mole]
$Nu$	— Nusselt number
$P$	— total pressure [Pa]
$P_m$	— mean vapour pressure [Pa]
$Pr$	— Prandtl number

$Q_s$	— sensible heat transfer [W/m <sup>2</sup> ]
$Q_v$	— latent heat transfer [kW/m <sup>2</sup> ]
$Q_c$	— conduction heat transfer [W/m <sup>2</sup> ]
$r$	— pore radius [m]
$R$	— gas constant [J/K.mol]
$Re$	— Reynolds number
$Ra$	— Rayleigh number
$T$	— absolute temperature [K]
$u$	— velocity [m/s]
$M_w$	— molecular weight of water [kg/mole]
$CM_{NaCl}$	— mole solute concentration [mole/L]
$T_f$	— bulk feed temperature
$T_{mf}$	— temperature at feed side membrane
$T_{mp}$	— temperature at coolant side membrane
$T_{cd}$	— temperature at the condensate
$T_p$	— temperature condensate plate-air gap
$T_{pc}$	— temperature at condensate plate-coolant
$T_c$	— bulk coolant temperature

### Subscripts and superscripts

a	— air
w	— water
f	— feed
m	— membrane
b	— bulk
mf	— feed side of membrane
mp	— coolant side of membrane
m	— mean; average
c	— coolant water
h	— hot region

### Greek letters

$\delta$	— membrane thickness; film thickness [m]
$\varepsilon$	— porosity
$\tau$	— tortuosity
$\mu$	— viscosity [N.s/m <sup>2</sup> ]
$\rho$	— density [kg/m <sup>3</sup> ]

### References

- [1] M.A. Dawoud, The role of desalination in augmentation of water supply in GCC countries, *Desalination* 186 (2005) 187–198.
- [2] Y. Lu, J. Chen, Optimal design of multistage membrane distillation systems for water purification, *Ind. Eng. Chem. Res.* 50 (2011) 7345–7354.
- [3] M.J. Abdulrazzak, The role of desalination in meeting water supply demands in Western Asia, *Water Int.* 27 (2002) 395–406.
- [4] A. Alkhdhiri, N. Darwish, N. Hilal, Membrane distillation: A comprehensive review, *Desalination* 287 (2012) 2–18.
- [5] A. Khalifa, Water and air gap membrane distillation for water desalination—An experimental comparative study, *Sep. Purif. Technol.* 141 (2015) 276–284.
- [6] M.N.A. Hawlader, R. Bahar, K.C. Ng, L.J.W. Stanley, Transport analysis of an air gap membrane distillation (AGMD) process, *Desalin. Water Treat.* 42 (2012) 333–346.
- [7] M. Khayet, T. Matsuura, *Membrane Distillation: Principles and Applications*, Elsevier B.V., Amsterdam, 2011.
- [8] F.A. Banat, J. Simandl, Desalination by membrane distillation: A parametric study, *Sep. Sci. Technol.* 33 (1998) 201–226.
- [9] B.L. Pangarkar, M. Sane, Performance of air gap membrane distillation for desalination of ground water and seawater, *Eng. Technol.* 75 (2011) 973–977.
- [10] D. Singh, K.K. Sirkar, Desalination by air gap membrane distillation using a two hollow-fiber-set membrane module, *J. Membr. Sci.* 421–422 (2012) 172–179.
- [11] M.C. de Andrés, J. Doria, M. Khayet, L. Peña, J.I. Mengual, Coupling of a membrane distillation module to a multieffect distiller for pure water production, *Desalination* 115 (1998) 71–81.
- [12] A.S. Jönsson, R. Wimmerstedt, A.C. Harrysson, Membrane distillation—A theoretical study of evaporation through microporous membranes, *Desalination* 56 (1985) 237–249.
- [13] G.L. Liu, C. Zhu, C.S. Cheung, C.W. Leung, Theoretical and experimental studies on air gap membrane distillation, *Heat Mass Transfer.* 34 (1998) 329–335.
- [14] R. Tian, H. Gao, X.H. Yang, S.Y. Yan, S. Li, A new enhancement technique on air gap membrane distillation, *Desalination* 332 (2014) 52–59.
- [15] J.G. Lee, W.S. Kim, Numerical study on multi-stage vacuum membrane distillation with economic evaluation, *Desalination* 339 (2014) 54–67.
- [16] J. Gilron, L. Song, K.K. Sirkar, Design for cascade of crossflow direct contact membrane distillation, *Ind. Eng. Chem. Res.* 46 (2007) 2324–2334.
- [17] E.K. Summers, J.H. Lienhard V, Cycle performance of multi-stage vacuum membrane distillation (MS-VMD) systems, *IDA World Congress on Desalination and Water Reuse*, Tianjin, China, 2013, REF: IDAWC/TIAN13-202.
- [18] D.U. Lawal, A.E. Khalifa, Flux prediction in direct contact membrane distillation, *Int. J. Mater., Mech. Manuf.* 2 (2014) 302–308.
- [19] S. Srisurichan, R. Jiratananon, A.G. Fane, Mass transfer mechanisms and transport resistances in direct contact membrane distillation process, *J. Membr. Sci.* 277 (2006) 186–194.
- [20] S. Kimura, S. Nakao, Transport phenomena in membrane distillation, *J. Membr. Sci.* 33 (1987) 285–298.
- [21] F.A. Banat, J. Simandl, Membrane distillation for dilute ethanol: Separation from aqueous streams, *J. Membr. Sci.* 163 (1999) 333–348.
- [22] L. Martínez, J.M. Rodríguez-Maroto, On transport resistances in direct contact membrane distillation, *J. Membr. Sci.* 295 (2007) 28–39.
- [23] F.A. Banat, J. Simandl, Theoretical and experimental study in membrane distillation, *Desalination* 95 (1994) 39–52.
- [24] A.M. Alklaibi, N. Lior, Transport analysis of air gap membrane distillation, *J. Membr. Sci.* 255 (2005) 239–253.